

Interferometric Ground Cancellation for Above Ground Biomass Estimation

Mauro Mariotti d'Alessandro¹, Member, IEEE, Stefano Tebaldini², Senior Member, IEEE,
Shaun Quegan³, Maciej J. Soja⁴, Member, IEEE, Lars M. H. Ulander⁵, Fellow, IEEE,
and Klaus Scipal⁶, Member, IEEE

Abstract—A new processing technique, i.e., ground cancellation, which removes the ground signal from a pair of interferometric synthetic aperture radar (SAR) images, is used to emphasize the response from above-ground targets. This technique is of particular interest when studying forest canopies using low-frequency signals able to reach the underlying ground, in which case the portion of the signal coming from the ground interferes with the recovery of information about the vegetation. We demonstrate that the power in ground-canceled P-band HV SAR data gives significantly higher correlations with above-ground biomass (AGB) than the interferometric images considered separately. In addition, a significant increase in the sensitivity of backscatter to AGB is observed. Ground-canceled power may then be modeled or regressed to estimate AGB; these possibilities are not discussed here as they will be the topic of forthcoming publications. The effectiveness of this technique is proven through simulations and analysis of real data gathered on tropical forests. The stability of the technique is analyzed under the digital terrain model and baseline control errors, and compensation strategies for these errors are presented.

Index Terms—Above-ground biomass (AGB), biomass, forest, interferometry, synthetic aperture radar (SAR), tomography, tropical.

I. INTRODUCTION

BIO MASS plays two fundamental roles in the global carbon cycle and, hence, in climate: 1) as a carbon source when it is destroyed during land use change or forest degradation and 2) as a carbon sink when photosynthesis removes carbon from the atmosphere and stores it in vegetation. For this reason, above-ground biomass (AGB) is recognized as an essential climate variable within the global climate observing system. This has motivated several studies that use remote sensing to estimate AGB at the continental scale [1]–[3] as this is the only viable means of acquiring wall-to-wall observations with such large coverage.

Manuscript received October 16, 2019; revised February 19, 2020; accepted February 23, 2020. Date of publication March 12, 2020; date of current version August 28, 2020. (Corresponding author: Mauro Mariotti d'Alessandro.)

Mauro Mariotti d'Alessandro and Stefano Tebaldini are with the Dipartimento di Elettronica Informazione e Bioingegneria, Politecnico di Milano, 20133 Milan, Italy (e-mail: mauro.mariotti@polimi.it).

Shaun Quegan is with the Centre for Terrestrial Carbon Dynamics, University of Sheffield, Sheffield S3 7RH, U.K.

Maciej J. Soja is with MJ Soja Consulting, Hobart, TAS 7000, Australia, and also with the University of Tasmania, Hobart, TAS 7001, Australia.

Lars M. H. Ulander is with the Department of Earth and Space Sciences, Chalmers University of Technology, 412 96 Gothenburg, Sweden.

Klaus Scipal is with the Mission Science Division, European Space Agency, 2200 AG Noordwijk, The Netherlands.

Color versions of one or more of the figures in this article are available online at <http://ieeexplore.ieee.org>.

Digital Object Identifier 10.1109/TGRS.2020.2976854

Tropical forests are of key importance in the carbon cycle because they contain more than 70% of the world's biomass [4]. As a result, numerous local studies have explored the estimation of AGB in such forests, using optical frequencies (and LiDAR) [5]–[9], hyperspectral data [5], and microwaves at X- [10]–[12], C- [6], [11], [13], and L-bands [10], [11], [14]. However, AGB can only be inferred indirectly from such measurements, and the data are affected by environmental factors that need to be accounted for in the AGB inversion. In addition, sensor limitations often prevent the development of unique relationships between measurements and AGB [15].

A new perspective is offered by synthetic aperture radar (SAR) tomography (TomoSAR), which allows focusing of the signal at specific elevations inside the vegetation layer. The joint use of TomoSAR and longer wavelengths (P-band, about 70 cm) gives access to the whole 3-D structure of forests; echoes coming from ground level up to the top of the canopy can be recorded and analyzed separately [16], [17]. The first research demonstrated that a layer centered at 30 m above ground level exhibits a high correlation with AGB [18]; in addition, it is shown that there is no saturation effect for AGB greater than 350 Mg/ha, unlike what is typically observed in the total forest return. Among several possible explanations for this [19], rejection of the ground return inherent to TomoSAR focusing is likely to play a key role. The ground echo is determined by many factors [20], [21], several of them are unrelated to AGB and are hard to model, such as double bounce and soil moisture variations. Canceling the ground return, therefore, simplifies the inversion and is likely to strengthen the relation between radar power and AGB; this is the primary motivation for this article. Ground cancellation, carried out here in its simplest form, uses just two radar images and does not rely on a model for either the ground or the forest layer. Hence, it overcomes one of the main obstacles of TomoSAR, which is the collection of a large number of interferometric acquisitions. Interferometric ground cancellation combines two coherent single look complex (SLC) images to achieve a dramatic reduction in the ground-to-volume ratio, thus easing the analysis of the vegetation canopy. This technique is derived and discussed in Section II. Section III shows its connection with AGB. In Section IV, some strategies to reduce the impact of topography and acquisition geometry are presented. Finally, Section V presents a discussion and overall conclusions.

II. INTERFEROMETRIC GROUND CANCELLATION

The ground cancellation technique combines two interferometric SAR (InSAR) images to suppress the signal coming from the ground and emphasize the signal coming from the above-mentioned vegetation layer. The idea behind ground cancellation can be described by using the well-known principles of InSAR processing; it also can be illustrated by analyzing the behavior of the SAR images in the frequency domain. Both approaches are shown in this section.

SARs are coherent imaging systems, i.e., they return both the amplitude and phase of the backscattered echo. The recorded signal is determined by the transmitted waveform, the characteristics of the medium through which it propagates, and the backscattering coefficient of the target. Delayed and scaled replicas of the transmitted signal are received along the trajectory followed by the sensor. The range compression operation converts the commonly used linear frequency-modulated signal into a narrower sinc-type response by matched filtering, thus discriminating targets in the range direction; the width of the main lobe is inversely proportional to the signal bandwidth and determines the range resolution of the system. Similarly, many echoes from the same target are collected as the sensor moves forward so that the information related to a single-point scatterer spreads across several data takes. Azimuth compression is needed to make all these echoes collapse in a small neighborhood and then achieving resolution capability along the direction identified by the flight direction. After range and azimuth compression, the signal gathered in each range line (constant azimuth) is determined by all the scattering targets that share the same azimuth coordinate; the echoes coming from every target in a small neighborhood of any range coordinate within this plane get coherently summed at the receiver. As a consequence, targets sharing the same azimuth and range coordinates cannot be distinguished in a single SLC image. The geometrical locus where these targets lie is a circle centered on the sensor trajectory and orthogonal to it. For practical reasons, this circle is often approximated with its tangent in correspondence of a reference target: the cross-range direction ν .

In order to be sensitive to the ν coordinate, InSAR systems [22] use an SLC pair (master and slave) with slightly different cross-range directions: ν_M and ν_S . Targets lying on the ν_M -axis in the first approximation feature the same distance from the master sensor but different from the slave. As a consequence, the phase delay due to wave propagation grows with ν and the growth rate is proportional to the tilt of ν_S with respect to ν_M . It follows that the phase difference between the master and slave acquisitions reveals the position of the scattering target along ν_M allowing the localization in the 3-D space.

In practice, two main processing steps come before the estimation of the interferometric phase: coregistration and phase flattening. The former step locally translates the slave image so that the same target appears in the same range azimuth coordinate in both images. The latter removes, from the interferometric phase, the value that it is expected from a target in a reference position; this operation shifts the origin of the cross-range axis in correspondence of the reference

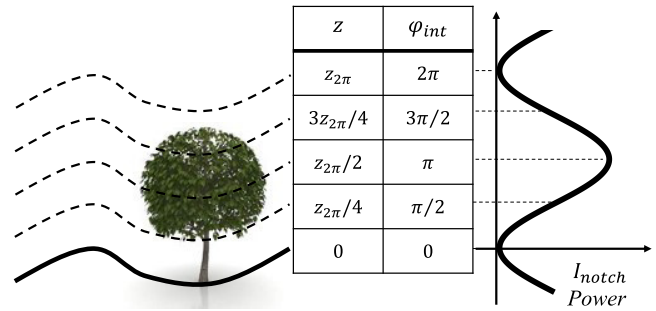


Fig. 1. Relationship between elevation, interferometric phase, and vertical power shaping provided by the interferometric ground cancellation processing chain. Targets lying at the ground level are associated with zero interferometric phases and are canceled by coherent subtraction.

target. After phase flattening, zero interferometric phases are measured for targets lying at the reference position, and the estimated elevations are intended relative to the reference target. Common choices for carrying out phase flattening are digital elevation models (DEMs) when available, otherwise flat surfaces. Whenever a digital terrain model (DTM) is used, the phase flattening processing step takes the origin of the cross-range axis in correspondence of the local ground level throughout the imaged scene; we refer to this operation as ground steering. Exploiting the link between ν and vertical (z)-axis, measurements in the master and slave images can be expressed as

$$I_M = \int a(z) \cdot dz \quad (1)$$

$$I_S = \int a(\zeta) \cdot e^{j \cdot k \cdot z \cdot \zeta} d\zeta \quad (2)$$

where $a(z)$ is the complex reflectivity density of the distributed target and kz is the phase-to-height conversion factor [22]. From now on, the SLC radar images are assumed to be focused, calibrated [23], coregistered, and ground steered.

We now define the radar image resulting from the difference between I_M and I_S as ground-notched image (I_{notch}). The power associated with each pixel of I_{notch} can be expressed as

$$\begin{aligned} E[|I_{notch}|^2] &= E\left[\left|\int a(z) \cdot dz - \int a(\zeta) \cdot e^{j \cdot k \cdot z \cdot \zeta} d\zeta\right|^2\right] \\ &= 2 \int \sigma_a^2(z) (1 - \cos(kz \cdot z)) dz \end{aligned} \quad (3)$$

where $a(z)$ has been assumed uncorrelated along z , i.e., $E[a(z)a^*(\zeta)] = \sigma_a^2(z) \cdot \delta(z - \zeta)$. Equation (3) states that the squared magnitude of the ground-notched image is given by the integral of the vertical reflectivity profile $\sigma_a^2(z)$ shaped by a sinusoid. This sinusoidal weighing eliminates the echoes coming from integer multiples of the ambiguity height and emphasizes intermediate values (see Fig. 1). Complete rejection is achieved only for targets at the elevation used when ground steering the SLCs, but the nearby heights suffer significant attenuation. It follows that the ground surface, even if it is flat, cannot be completely removed from the data as it spreads over a small, yet finite, angular range $\delta\vartheta$, i.e., a finite vertical range in accordance with the side-looking

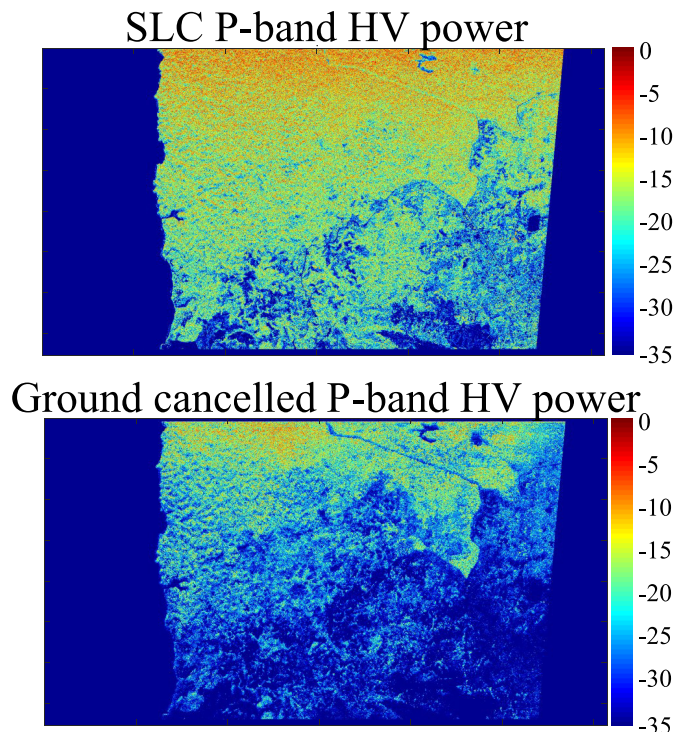


Fig. 2. (Top) Estimated SLC radar power [dB] in the HV polarimetric channel. (Bottom) Estimated power [dB] of the corresponding ground-canceled image obtained, as described in Section II. Areas covered by dense or high trees stand out after ground cancellation. Images drawn from the Mondah data set acquired by DLR during the AfriSAR 2016 [24], [25] campaign.

SAR imaging geometry. The non-zero extension of the ground surface means that the spectral components illuminated by the master and slave acquisitions do not completely overlap. The part of the spectrum not shared by the two received signals cannot be removed by coherent subtraction and represents the residual power coming from the canceled ground. An example of the ground-canceled power is shown in the bottom image of Fig. 2; the corresponding SLC power is shown in the top image for comparison.

Fig. 3 shows the spectral properties in the range direction of two interferometric SLCs; noise-free acquisitions on the bare ground were simulated with 60-m ambiguity height on a 10° tilted surface. The top image of Fig. 3 shows the baseband spectra associated with the master and slave images. The middle image shows the same spectra after ground steering; the two spectra are no longer centered around zero, but the common frequencies are aligned. The ground steering step is equivalent to compensation of the spectral shift, as described in [26]. The bottom image of Fig. 3 shows that in the frequency domain, the residual notched power is due to the extreme parts of the ground spectrum illuminated either by the master sensor or the slave sensor. These spectral components can be determined using the acquisition geometry and the system parameters and could be filtered out at the expense of resolution loss in the ground-notched image. Furthermore, the strongest contribution from ground level when gathering data on forests is often due to the double-bounce scattering mechanism [20], [27]. A vertical tree trunk over flat ground

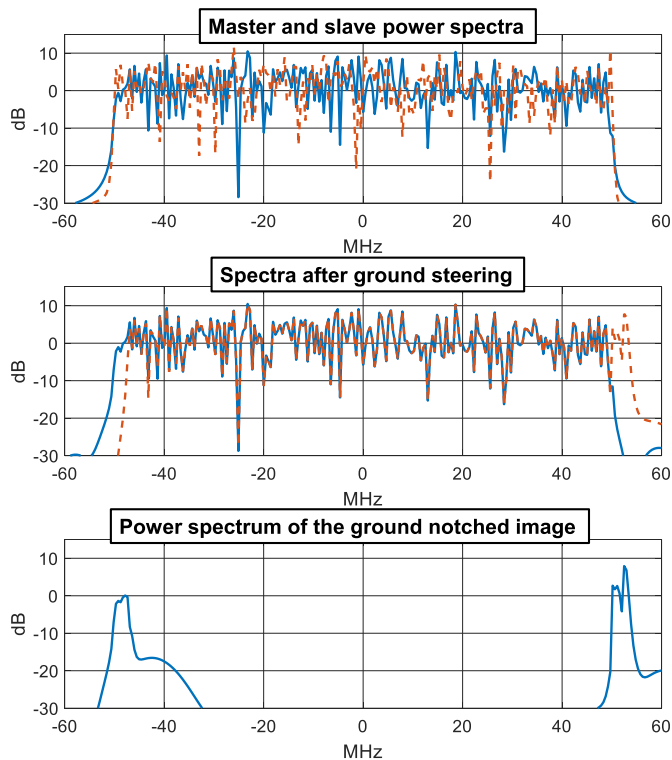


Fig. 3. (Top) Simulated power spectrum of two InSAR acquisitions for a single azimuth position; only bare soil was simulated. (Middle) Same spectra after the ground steering processing step. (Bottom) Spectrum of the ground-notched image. Spectral components shared by the two acquisitions are canceled after coherent subtraction.

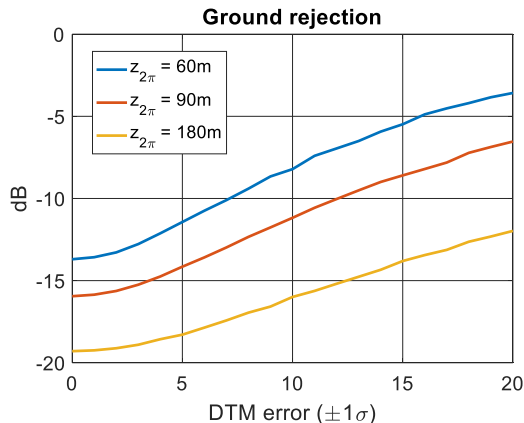


Fig. 4. Rejection of the ground echo as a function of the inaccuracy of the DTM used for the ground steering step; Gaussian noise is simulated, whose standard deviation increases along the x -axis. Results associated with three different heights of ambiguity are plotted.

acts like a dihedral whose phase center lies at the base of the tree and so reflects back most of the signal energy. The features of this scattering mechanism are closer to that of a point-like scatterer than an extended target, making spectral filtering less appropriate.

The signal backscattered by the ground may also be different in the two images if their acquisitions are separated by a significant amount of time. In this case, physical changes might have occurred in the soil producing temporal decorrelation and degrading the quality of the coherent cancellation. This issue has been described in [29].

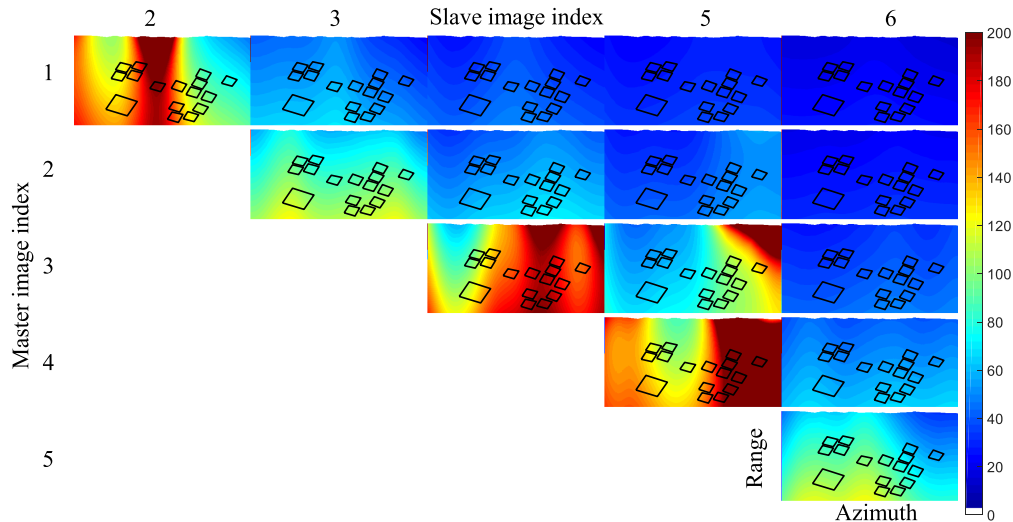


Fig. 5. Spatial distribution of the height of ambiguity ($z_{2\pi} = 2\pi/kz$) for each pair of the TropiSAR data set (Paracou site [28]). It corresponds to the elevation of the first zero of the sinusoid weighing the vertical reflectivity profile of the forest shown in (3).

A. Errors in the DTM

Any discrepancies between the available DTM and the true topography lead to flawed ground cancellation. According to the analysis given in this section, this can be described in either the spatial or wavenumber domain. Errors in the DTM induce translations in the I_{notch} power function of Fig. 1; the reference height is set away from ground level so that the ground signal is no longer zero-weighted. In the frequency domain, this amounts to a mismatch between the two spectra shown in the middle image of Fig. 3; this misalignment prevents the common spectral components from being completely rejected, thus allowing residual power to come from the ground level. This residual ground power has been quantified using numerical analysis considering both baseline (through the ambiguity height) and DTM errors. The curves shown in Fig. 4 were obtained by simulating a pair of InSAR acquisitions on bare flat ground for three different values of the height of ambiguity: 60, 90, and 180 m. Ground steering was carried out with the true DTM corrupted by the zero-mean Gaussian noise with a standard deviation ranging from 0 to 20 m. The y-axis shows the ratio between the power of the ground-notched image and the power of one of the SLCs involved.

III. CORRELATION WITH AGB

The processing chain described in Section II returns a complex image mainly determined by targets that lie above ground level. Hence, the power associated with the ground canceled image is expected to show improved correlation with AGB; this is demonstrated below using data from the 2009 TropiSAR campaign [28], [30]. The tomographic stack consists of six fully polarimetric SLC images acquired over the area surrounding Paracou in French Guiana. The spatial baseline increases almost monotonically with the image index so that kz depends approximately only on the difference between indices. The vertical shaping introduced by the interferometric ground cancellation can be obtained based on these

phase-to-height conversion factors, as shown in Fig. 5. Ground measurements of AGB are also available at this site; 16 plots have been monitored since the 1980s and provide excellent estimates of the true AGB. The 16 regions of interest (ROIs) considered here are 15 squares of 6.25 ha ($250 \times 250 \text{ m}^2$) and 1 square of 25 ha ($500 \times 500 \text{ m}^2$); forest inventory was carried out in 2009 when the SAR survey took place. Please refer to [18] and [30]–[32] for a description of the site and *in situ* AGB measurements.

The availability of six coherent images allows $6(6-1)/2 = 15$ ground-notched images to be built, each emphasizing a different elevation above the ground but still rejecting the ground return. The ground-notched power with overlapped the 16 ROIs is shown in Fig. 6 for each image pair. The effectiveness of the ground cancellation regardless of the spatial baseline can be demonstrated by examining the copolar phase difference, i.e., the difference between the phases of the HH and VV polarimetric channels. This is expected to be near 0° for single-bounce scattering (direct return from the ground or volume scattering) and approaches 180° for double-bounce scattering. Over forests, the double bounce is mainly due to double reflection from the ground and trunks, and its phase center is located at the ground level [20]. The copolar phases associated with a single SLC image together with 0-m tomographic signal, short baseline notching (combining images 1 and 2), and long-baseline notching (images 1 and 6) are shown in Fig. 7. There are no significant differences between the notched images in terms of ground cancellation, so all of them appear viable candidates for estimating AGB.

However, different image pairs provide different weighing of the vertical reflectivity profile. Using diagrams similar to Fig. 1 for each panel in Fig. 5, it is possible to determine which parts of the vegetation layer are emphasized or nullified. The associated modification of the sensitivity to AGB was evaluated by plotting the power in the HV channel in each ground-notched image (after compensating by a simple $\sin(\vartheta - \alpha)$ factor [18], where α is the ground slope in the

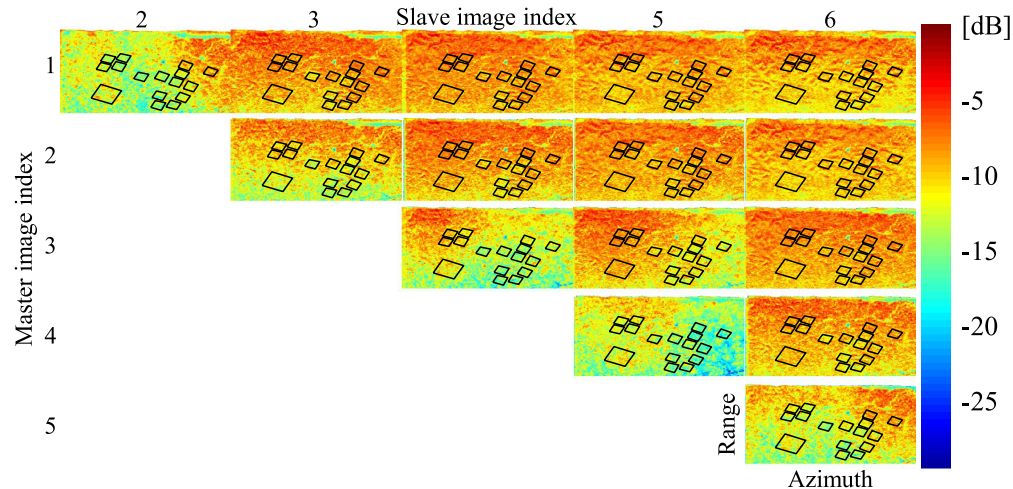


Fig. 6. Power of the ground-notched images for each pair of the TropiSAR data set (Paracou site [28]); images have been cropped to focus on the regions where *in situ* AGB measurements are available. Measured power has been corrected by a $\sin(\vartheta - \alpha)$ factor to account for the acquisition geometry.

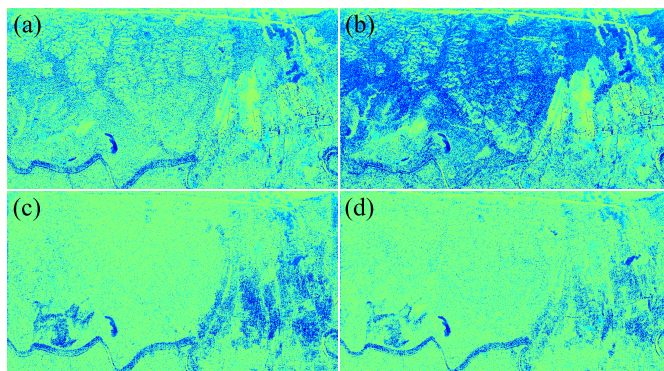


Fig. 7. Copolar phase (φ_{cop}) associated with (a) SLC, (b) 0-m tomography, (c) short-baseline ground notch (images 1 and 2), and (d) long-baseline ground notch (images 1 and 6). Dark blue: $\varphi_{\text{cop}} \approx \pm 180^\circ$. Light green: $\varphi_{\text{cop}} \approx 0^\circ$.

range direction and the corresponding in azimuth is neglected) against AGB from ground measurements. Fig. 8 shows the improvement when moving from a single SLC image to two images processed according to the ground notching technique. Whenever *in situ* AGB is available, the line of best fit is overlapped, from which we can the Pearson correlation coefficient and the sensitivity of the radar power to AGB. Sensitivity is expressed in (Mg/ha)/dB, i.e., the increase in AGB yielding an increment of 1 dB of power. The improvement when moving from one to two SAR images is clear; the unnotched backscattered power is poorly correlated with and has almost no sensitivity to AGB, while the AGB can readily be estimated from the ground-notched power [25]. The values of the correlation and sensitivity to AGB of the ground-notched power for each HV image pair in the TropiSAR data set are shown in Fig. 9 as blue bars (leftmost ones). Note that smaller sensitivity values are preferable as they give more accurate estimates of AGB when inverting the regression relations. It can be seen that the HV power is positively correlated with AGB for almost every notched image, but there are large fluctuations in the sensitivity. These are driven by three main factors: one biophysical and two related to the acquisition geometry. The biophysical factor arises from

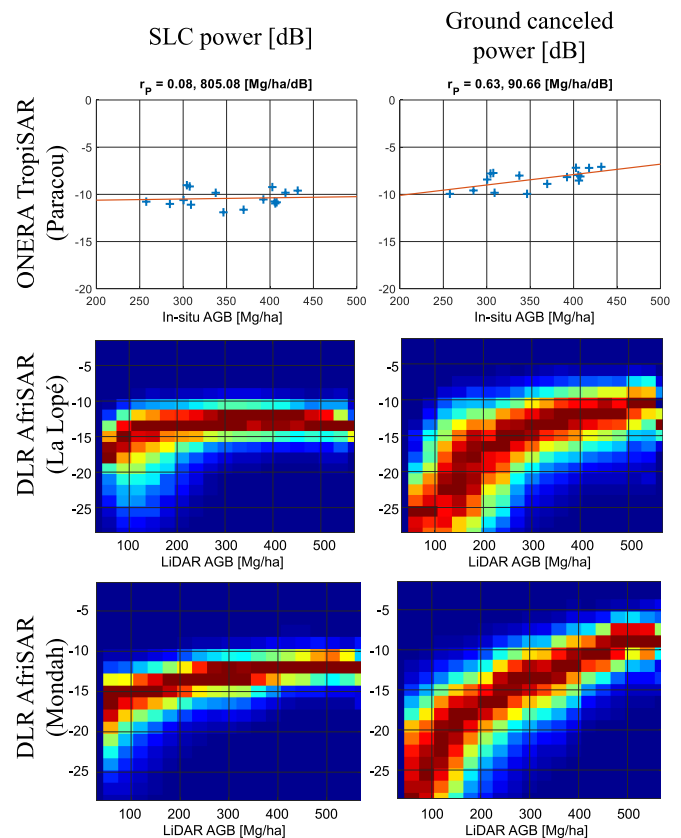


Fig. 8. Relation between AGB and radar HV power. (Left) Power of a single SLC image is considered. (Right) Ground canceled power. The impact of the geometry of acquisition has been mitigated through the factor $\sin(\vartheta - \alpha)$. Images 1 and 3 of the TropiSAR [30] data set have been used to generate the top right image; AfriSAR [24], [25], [31] ground-notched images are associated with a height of ambiguity of about 150 m.

the vertical structure of the vegetation, and in particular, how well-correlated the tree components lying around 30 m above the ground is with the total AGB. Previous works [18], [19] indicate that these parts of the tree are tightly linked to the total AGB amount. Hence, the spatial baseline separating the two SLC images should be chosen to emphasize the backscatter

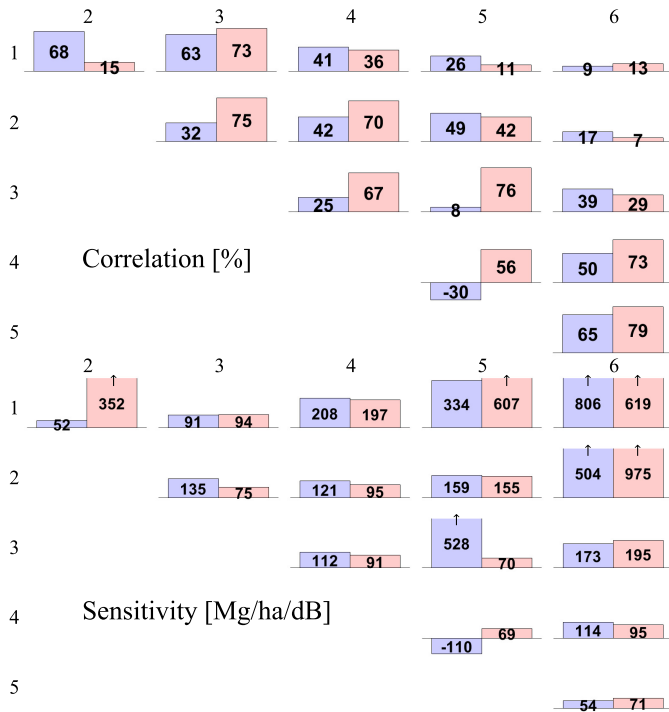


Fig. 9. Correlation and sensitivity to reference *in situ* AGB of (Left, blue) ground-canceled P-band HV power corrected by a $\sin(\vartheta - \alpha)$ factor and (Middle, red) ground-canceled P-band HV power corrected using the procedure described in Section IV. Image indexes are shown on top and on the left; all available image pairs are considered. An upward arrow states that the height of the bar was cropped for visualization purpose.

from this height. Both factors arising from the acquisition geometry relate to the baseline. Very large baselines lead to fast shaping (see I_{notch} power in Fig. 1) in the vertical direction, which means that a smaller fraction of the ground return is rejected when there are significant slopes. In principle, ground cancellation with very long baselines is more vulnerable to errors in the DTM, as shown in Fig. 4. However, this is expected to have little impact as the accuracy of the DTM used here is assessed to be about 2 m [33]. Imperfect control of the platform also has consequences since spatially varying oscillations of the normal baseline will cause different vertical weighing in different areas. In this case, the power associated with the ground-notched image becomes correlated with the height of ambiguity. The power fluctuations due to the spatial variations of the normal baseline may be erroneously ascribed to AGB variability. This feature can be immediately appreciated by comparing the maps showing the height of ambiguity in Fig. 5 to the power maps shown in Fig. 6. Most of the spatial fluctuations of the ground-notched power can be explained by the variability of the normal baseline. However, this dependence of the ground-notched power on the acquisition geometry and topography can be taken into account, as shown in Section IV.

IV. EQUALIZED GROUND CANCELLATION

When transferring the findings from Section III to a spaceborne case, two main effects need to be taken into account: 1) the variability of the incidence angle from near to far range and 2) the stability of the sensor trajectory. In airborne

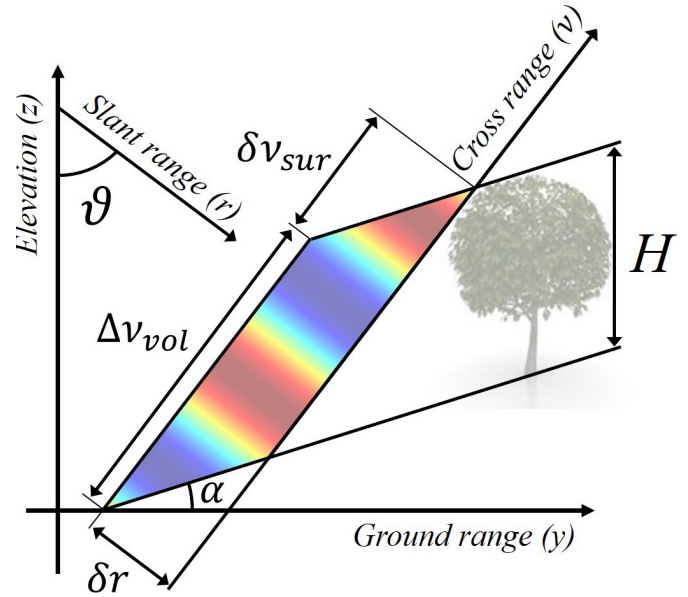


Fig. 10. Reference geometry for the computation of the theoretical ground canceled power. The oscillating function (ranging from 0 to 4) introduced by the interferometric processing is integrated over the sketched parallelogram [region Ω in (4)].

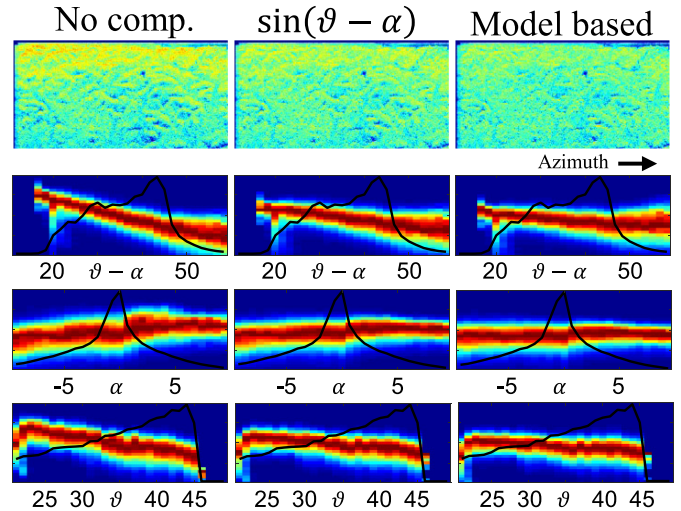


Fig. 11. Comparison between different strategies for mitigating the impact of the acquisition geometry on the ground-canceled power. The bivariate histograms show the relationship between the power maps and geometric parameters. (From Top to Bottom) Incidence angle ($\vartheta - \alpha$), ground slope (α), and look angle (ϑ). The peak value of each column of the histograms has been normalized to 1; the black lines show a scaled version of the marginal distribution of the angles here shown. The model-based equalization is described in Section IV.

data, the incidence angle can range from 15° to 60° or more, as opposed to a few degrees for spaceborne images. The ideal linear trajectory is also more difficult to follow for an airplane because of the turbulence in the atmosphere at lower altitudes [23]. Both these issues affect interferometric ground cancellation by causing the perpendicular baseline to change along both range and azimuth, leading to spatial variations in the height of ambiguity. This, in turn, causes spatial oscillation in the ground-notched power. In the following, a method to reduce the impact of the acquisition geometry is presented. It is based on theoretical computation of the ground-canceled

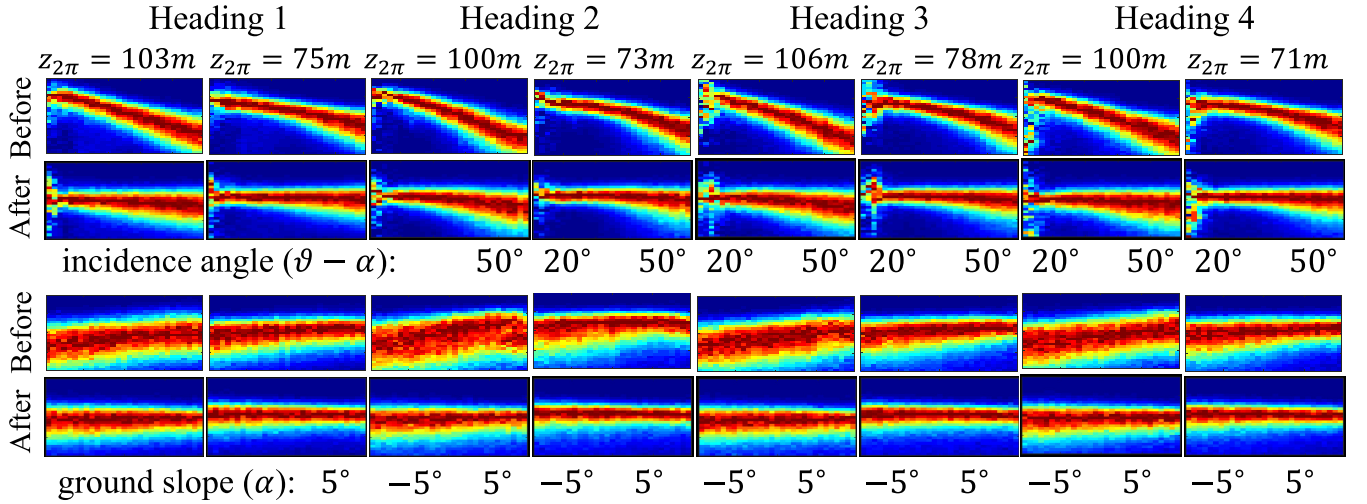


Fig. 12. Dependence on the ground slope and incidence angle of the ground-canceled power (y-axis) before and after the model-based equalization described in Section IV. The removal of most of the dependence on the acquisition geometry is witnessed by significantly flatter histograms. Data come from the DLR AfriSAR campaign over La Lopé [24], [25]; three SLC images were available from each of four headings.

power given the actual geometry and a simple reference model of the forest layer. The measured power is then divided by this theoretical power, resulting in a normalized value little affected by the acquisition geometry.

The computation of the theoretical ground-canceled power is based on a simple distribution of elementary scattering targets, equivalent to a uniform layer from 0 to H meters with respect to the local ground level. Each scattering target within the resolution cell is assumed to contribute equally to the backscattered power. The effect of the interferometric ground cancellation is to weight these power contributions according to their cross-range coordinate and the phase-to-height conversion factor. For the computation of the normalizing factor, a fixed value of 30 m has been chosen for H . Analysis has shown that this value is not critical; any value between 20 and 40 m may be used as long as it is kept fixed for the whole scene. Fig. 10 shows the reference geometry for the computation of the ground canceled power. The resolution cell is bounded by the resolution (δr) in slant range and by the forest top layer in the cross range. This 2-D region (Ω) defines the boundary for the integration of the weight provided by the ground notching

$$P_{\text{theo}} = \iint_{\Omega} (1 - \cos(kv \cdot v)) dv dr. \quad (4)$$

The phase-to-cross-range scaling factor has been used here because the standard kz definition does not take into account the ground slope; it is defined as

$$kv = kz \cdot \sin \vartheta. \quad (5)$$

The spread of the target distribution along the cross-range can be ascribed to the limited bandwidth of the system and to the extent of the vegetation layer. They are referred to as δv_{sur} and Δv_{vol} , respectively

$$\delta v_{\text{sur}} = \delta r \cdot \frac{1}{\tan(\vartheta - \alpha)} \quad (6)$$

$$\Delta v_{\text{vol}} = H \cdot \frac{\cos \alpha}{\sin(\vartheta - \alpha)}. \quad (7)$$

The integral in (4) can be solved in the closed form

$$P_{\text{theo}} = 2(\Delta v_{\text{vol}} + \delta v_{\text{sur}}) \cdot \left(1 - \frac{\sin(kv(\Delta v_{\text{vol}} + \delta v_{\text{sur}}/2)) + \sin(kv \cdot \delta v_{\text{sur}}/2)}{kv(\Delta v_{\text{vol}} + \delta v_{\text{sur}})} \right). \quad (8)$$

The volumetric compensation expressed by (8) has been used to remove the dependence on the acquisition geometry and topography from several data sets. Its effects for P-band HV data from the Paracou data set of the ONERA TropiSAR 2009 campaign and the La Lopé data set of the DLR AfriSAR 2016 campaign [24], [25] are shown in Figs. 11 and 12, respectively. These histograms show how effective this approach is in removing the correlation with the main geometrical parameters. After the proposed normalization, the ground-notched power does not significantly depend on geometrical quantities resulting in almost flat bivariate histograms.

The sensitivity and correlation to AGB of the ground-notched power after this model-based equalization are shown by the rightmost (red background) bars of Fig. 9 for the Paracou site. Despite using a simple reflectivity profile, the improvement is clear (compared with the leftmost bars in Fig. 9). Most of the pairs exhibit high correlation and sensitivity to AGB after the compensation; only image pair 1 & 2 have significantly reduced performance. This would be expected given the corresponding map of the height of ambiguity, as shown in Fig. 5. Trajectories are often very close or even crossing, so most of the energy coming from the forest canopy are rejected, not just that from the ground. In this case, compensation cannot succeed as the SNR is very low, and any *a posteriori* amplification would emphasize noise. This must also be kept in mind when interpreting pairs 3 & 4 and 4 & 5. Step-2 pairs (1 & 3, 2 & 4, 3 & 5, and 4 & 6) exhibit the best correlation and sensitivity. Their pairwise baseline distribution emphasizes the scatterers placed around 30 m, as shown in Fig. 5. A further increase of the baseline leads to a progressive decrease in the correlation with AGB, as shown in the top right part of Fig. 9.

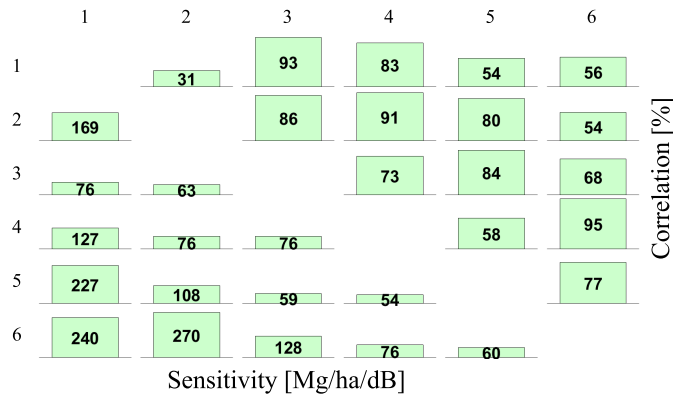


Fig. 13. Sensitivity and correlation to *in situ* AGB of the ground-canceled power after empirical removal of the dependence on the acquisition geometry (see Section IV-A).

A. Note on Equalization

Section IV presented a method to cope with space-varying acquisition geometry and topography that is useful for interpreting the ground-canceled power. This method relies on a simple physical model of the backscattered power and is able to remove most of the correlation with geometrical parameters. However, on the Paracou data set, a $1/\sin(\vartheta - \alpha)$ factor further reduced the correlation of the ground-canceled power with the acquisition geometry. At the same time, both the correlation with *in situ* AGB and the sensitivity to AGB increased. They are both high for most pairs, and they follow a reasonable (also shown in Fig. 13) pattern; step-1 pairs are affected by large fluctuations and their values are noisy, while toward longer baselines (further from the main diagonal); the performance decreases. The correlation and sensitivity of the step-2 pairs (emphasizing targets at about 30 m) are excellent.

V. CONCLUSION AND DISCUSSION

This article presents a new technique for estimating AGB from a pair of InSAR images referred to as interferometric ground cancellation since it rejects the signal coming from ground level. Its rationale is that the ground-level signal is affected by AGB but includes several extraneous contributions that hinder the estimation of AGB, and hence, it should be removed when possible. The ground cancellation process emphasizes scattering objects located around a specific elevation above the ground, determined by the normal baseline. Significantly improved correlations with AGB are observed for most baseline cases, and the highest correlations are reached for pairs with a height of ambiguity of about 60 m, emphasizing targets at 30 m above the terrain. In order to achieve the best correlations, the impact of the acquisition geometry on the ground-canceled power must be minimized. To achieve this, a normalizing factor has been derived based on a simple physical model; this yields a correlation of about $r_p = 0.75$ and sensitivity to AGB of 90 Mg/ha/dB. It remains to be seen if a better characterization of the vertical structure of the forest gained, for example, from tomography leads to further improvement.

For the Paracou site, $r_p = 0.95$ and 77 Mg/ha/dB can be obtained by resorting to an empirical minimization of the

impact of the acquisition geometry on the ground-canceled power. While the optimal strategy for calibrating ground-canceled power is still an open question, these results clearly demonstrate the effectiveness of the interferometric ground cancellation; power coming from the ground level is minimized, and this results in significantly higher sensitivity to AGB.

These results have been obtained by processing the P-band data. However, no limitations exist for this technique to be applied to measurements gathered at different central frequencies. The L-band signals are widely used for the exploration of vegetated areas too although their penetration is smaller. In general, higher frequencies experience a stronger attenuation, thus reducing the backscattered intensity coming from the ground beneath. For this reason, the ground cancellation technique is more suited when working with longer wavelengths. Nevertheless, the wavelength must be compared with the total attenuation provided by the vegetation layer, that is, this technique is expected to strongly improve the results whenever the thickness of the vegetation layer does not prevent the signal from reaching the underlying ground.

The quantity used here to estimate AGB is simply the ground-canceled HV power, but combining this with other observables, including the ground-canceled HH and VV power and forest height, might lead to better and more robust performance. In addition, spectral shift filtering should further improve the effectiveness of the ground cancellation by removing the spectral components of the ground that cannot be canceled by coherent combination. The ground cancellation technique allows the emphasis of scattering regions at different heights, as done by tomography. The vertical resolution is coarser than for TomoSAR, but only a pair of coherent images are needed, rather than a whole stack. This is particularly valuable when dealing with repeat-pass surveys as it significantly relaxes the constraint on temporal decorrelation of the target. Also, AGB estimates can be produced more frequently, leading to faster response to changes. Hence, the algorithm proposed here is likely to form a key element in processing the data from the interferometric phase of the ESA BIOMASS mission, whose launch is planned for 2022.

REFERENCES

- [1] S. S. Saatchi *et al.*, "Benchmark map of forest carbon stocks in tropical regions across three continents," *Proc. Nat. Acad. Sci. USA*, vol. 108, no. 24, pp. 9899–9904, May 2011. [Online]. Available: <http://www.pnas.org/content/108/24/9899.abstract>
- [2] M. Santoro *et al.*, "Forest growing stock volume of the northern hemisphere: Spatially explicit estimates for 2010 derived from ENVISAT ASAR," *Remote Sens. Environ.*, vol. 168, pp. 316–334, Oct. 2015. [Online]. Available: <http://www.sciencedirect.com/science/article/pii/S003442571530064X>
- [3] V. Avitabile *et al.*, "An integrated pan-tropical biomass map using multiple reference datasets," *Global Change Biol.*, vol. 22, no. 4, pp. 1406–1420, Jan. 2016, doi: [10.1111/gcb.13139](https://doi.org/10.1111/gcb.13139).
- [4] Y. Pan *et al.*, "A large and persistent carbon sink in the world's forests," *Science*, vol. 333, no. 6045, pp. 988–993, 2011. [Online]. Available: <https://science.sciencemag.org/content/333/6045/988>
- [5] G. Vaglio Laurin *et al.*, "Above ground biomass estimation in an african tropical forest with lidar and hyperspectral data," *ISPRS J. Photogram. Remote Sens.*, vol. 89, pp. 49–58, Mar. 2014. [Online]. Available: <http://www.sciencedirect.com/science/article/pii/S0924271614000045>

- [6] S. M. Ghosh and M. D. Behera, "Aboveground biomass estimation using multi-sensor data synergy and machine learning algorithms in a dense tropical forest," *Appl. Geography*, vol. 96, pp. 29–40, Jul. 2018. [Online]. Available: <http://www.sciencedirect.com/science/article/pii/S0143622818303114>
- [7] C. A. Silva *et al.*, "Comparison of Small- and large-footprint lidar characterization of tropical forest aboveground structure and biomass: A case study from central gabon," *IEEE J. Sel. Topics Appl. Earth Observ. Remote Sens.*, vol. 11, no. 10, pp. 3512–3526, Oct. 2018.
- [8] M. N. Bazezew, Y. A. Hussin, and E. H. Kloosterman, "Integrating airborne LiDAR and terrestrial laser scanner forest parameters for accurate above-ground biomass/carbon estimation in Ayer Hitam tropical forest, Malaysia," *Int. J. Appl. Earth Observ. Geoinformation*, vol. 73, pp. 638–652, Dec. 2018. [Online]. Available: <http://www.sciencedirect.com/science/article/pii/S030324341830727X>
- [9] P. Ploton *et al.*, "Toward a general tropical forest biomass prediction model from very high resolution optical satellite images," *Remote Sens. Environ.*, vol. 200, pp. 140–153, Oct. 2017. [Online]. Available: <http://www.sciencedirect.com/science/article/pii/S0034425717303553>
- [10] S. Enghart, V. Keuck, and F. Siegert, "Modeling aboveground biomass in tropical forests using multi-frequency SAR data—A comparison of methods," *IEEE J. Sel. Topics Appl. Earth Observ. Remote Sens.*, vol. 5, no. 1, pp. 298–306, Feb. 2012.
- [11] U. Khatri, G. Singh, and S. Kumar, "Potential of space-borne PolInSAR for forest canopy height estimation over India—A case study using fully polarimetric L-, C-, and X-band SAR data," *IEEE J. Sel. Topics Appl. Earth Observ. Remote Sens.*, vol. 11, no. 7, pp. 2406–2416, Jul. 2018.
- [12] R. Treuhaft *et al.*, "Tropical-forest biomass estimation at X-Band from the spaceborne TanDEM-X interferometer," *IEEE Geosci. Remote Sens. Lett.*, vol. 12, no. 2, pp. 239–243, Feb. 2015.
- [13] M. L. R. Sarker, J. Nichol, H. B. Iz, B. B. Ahmad, and A. A. Rahman, "Forest biomass estimation using texture measurements of high-resolution dual-polarization C-Band SAR data," *IEEE Trans. Geosci. Remote Sens.*, vol. 51, no. 6, pp. 3371–3384, Jun. 2013.
- [14] R. K. Ningthoujam, P. K. Joshi, and P. S. Roy, "Retrieval of forest biomass for tropical deciduous mixed forest using ALOS PAL-SAR mosaic imagery and field plot data," *Int. J. Appl. Earth Observ. Geoinf.*, vol. 69, pp. 206–216, Jul. 2018. [Online]. Available: <http://www.sciencedirect.com/science/article/pii/S0303243418301120>
- [15] T. R. Feldpausch *et al.*, "Height-diameter allometry of tropical forest trees," *Biogeosciences*, vol. 8, no. 5, pp. 1081–1106, 2011. [Online]. Available: <https://www.biogeosciences.net/8/1081/2011/>
- [16] S. Tebaldini and F. Rocca, "Multibaseline polarimetric SAR tomography of a Boreal forest at P- and L-bands," *IEEE Trans. Geosci. Remote Sens.*, vol. 50, no. 1, pp. 232–246, Jan. 2012.
- [17] S. Tebaldini, D. Ho Tong Minh, M. Mariotti d'Alessandro, L. Villard, T. Le Toan, and J. Chave, "The status of technologies to measure forest biomass and structural properties: State of the art in SAR tomography of tropical forests," *Surv. Geophys.*, vol. 40, no. 4, pp. 779–801, May 2019, doi: [10.1007/s10712-019-09539-7](https://doi.org/10.1007/s10712-019-09539-7).
- [18] D. Ho Tong Minh, T. L. Toan, F. Rocca, S. Tebaldini, M. M. d'Alessandro, and L. Villard, "Relating P-Band synthetic aperture radar tomography to tropical forest biomass," *IEEE Trans. Geosci. Remote Sens.*, vol. 52, no. 2, pp. 967–979, Feb. 2014.
- [19] V. Meyer *et al.*, "Canopy area of large trees explains aboveground biomass variations across neotropical forest landscapes," *Biogeosciences*, vol. 15, no. 11, pp. 3377–3390, Jun. 2018. [Online]. Available: <https://www.biogeosciences.net/15/3377/2018/>
- [20] M. M. D'Alessandro, S. Tebaldini, and F. Rocca, "Phenomenology of ground scattering in a tropical forest through polarimetric synthetic aperture radar tomography," *IEEE Trans. Geosci. Remote Sens.*, vol. 51, no. 8, pp. 4430–4437, Aug. 2013.
- [21] M. J. Soja, G. Sandberg, and L. M. H. Ulander, "Regression-based retrieval of boreal forest biomass in sloping Terrain using P-band SAR backscatter intensity data," *IEEE Trans. Geosci. Remote Sens.*, vol. 51, no. 5, pp. 2646–2665, May 2013.
- [22] R. Bamler and P. Hartl, "Synthetic aperture radar interferometry," *Inverse Problems*, vol. 14, no. 4, pp. R1–R54, Aug. 1998. [Online]. Available: <https://iopscience.iop.org/article/10.1088/0266-5611/14/4/001/pdf>, doi: [10.1088/0266-5611/14/4/001](https://doi.org/10.1088/0266-5611/14/4/001).
- [23] S. Tebaldini, F. Rocca, M. Mariotti d'Alessandro, and L. Ferro-Famil, "Phase calibration of airborne tomographic SAR data via phase center double localization," *IEEE Trans. Geosci. Remote Sens.*, vol. 54, no. 3, pp. 1775–1792, Mar. 2016.
- [24] I. Hajnsek *et al.*, "Technical assistance for the development of airborne sar and geophysical measurements during the afrisar experiment," German Aerosp. Center (DLR), Cologne, Germany, Final Rep., 2011, vol. 1.
- [25] M. J. Soja *et al.*, "Above-ground biomass estimation with ESA's 7th Earth explorer mission biomass: Algorithm basics and performance over tropical forests," *Remote Sens. Environ.*, to be published.
- [26] F. Gatelli, A. M. Guamieri, F. Parizzi, P. Pasquali, C. Prati, and F. Rocca, "The wavenumber shift in SAR interferometry," *IEEE Trans. Geosci. Remote Sens.*, vol. 32, no. 4, pp. 855–865, Jul. 1994.
- [27] M. M. D'Alessandro and S. Tebaldini, "Phenomenology of P-Band scattering from a tropical forest through three-dimensional SAR tomography," *IEEE Geosci. Remote Sens. Lett.*, vol. 9, no. 3, pp. 442–446, May 2012.
- [28] P. Dubois-Fernandez *et al.*, "TropiSAR, a SAR data acquisition campaign in French Guiana," in *Proc. 8th Eur. Conf. Synth. Aperture Radar*, Jun. 2010, pp. 1–4.
- [29] M. M. d'Alessandro, Y. Bai, and S. Tebaldini, "Temporal stability of ground notched images," in *Proc. IEEE Int. Geosci. Remote Sens. Symp. (IGARSS)*, Jul. 2019, pp. 2387–2390.
- [30] P. Dubois-Fernandez *et al.*, "Technical assistance for the development of airborne sar and geophysical measurements during the tropisar 2009 experiment," Université Paul Sabatier, CIRAD, Toulouse, France, Final Rep., V2.1, Feb. 2011.
- [31] N. Labriere *et al.*, "In situ reference datasets from the TropiSAR and AfriSAR campaigns in support of upcoming spaceborne biomass missions," *IEEE J. Sel. Topics Appl. Earth Observ. Remote Sens.*, vol. 11, no. 10, pp. 3617–3627, Oct. 2018.
- [32] P. C. Dubois-Fernandez *et al.*, "The TropiSAR airborne campaign in french guiana: Objectives, description, and observed temporal behavior of the backscatter signal," *IEEE Trans. Geosci. Remote Sens.*, vol. 50, no. 8, pp. 3228–3241, Aug. 2012.
- [33] M. M. D'Alessandro and S. Tebaldini, "Digital terrain model retrieval in tropical forests through P-band SAR tomography," *IEEE Trans. Geosci. Remote Sens.*, vol. 57, no. 9, pp. 6774–6781, Sep. 2019.



Mauro Mariotti d'Alessandro (Member, IEEE) was born in Milan, Italy, in 1983. He received the bachelor's, master's, and Ph.D. degrees in telecommunications engineering from the Politecnico di Milano, Milan, in 2005, 2009, and 2014, respectively.

From 2014 to 2016, he was with the research team of CONAE, Buenos Aires, Argentina. Since 2016, he has been a Research Assistant with the Department of Electronics, Informatics and Bioengineering (DEIB), Politecnico di Milano. He worked on the development of the SAOCOM mission and bistatic configurations. He is currently working on the development of algorithms for the ESA BIOMASS systems. His research interests include synthetic aperture radar (SAR) tomography, interferometry, polarimetry, and calibration of airborne and spaceborne data.



Stefano Tebaldini (Senior Member, IEEE) received the M.S. degree in telecommunication engineering and the Ph.D. degree from the Politecnico di Milano, Milan, Italy, in 2005 and 2009, respectively.

Since 2005, he has been with the Digital Signal Processing Research Group, Politecnico di Milano, where he currently an Associate Professor. He has been a Key Scientist in several studies with the European Space Agency (ESA), Paris, France, concerning the tomographic phase of the BIOMASS Mission. He was a member of the SAOCOM-CS Expert Group, ESA. He is one of the inventors of a new technology patented by T.R.E. for the exploitation of multiple interferograms in the presence of distributed scattering. He teaches courses on signal theory and remote sensing at the Politecnico di Milano. His research interests include earth observation with synthetic aperture radar (SAR) and radar design and processing.



Shaun Quegan is currently a Professor with the University of Sheffield, Sheffield, U.K., and a member of the National Centre for Earth Observation. His research over the last 25 years has been mainly concerned with using satellite data and ecosystem models to clarify the role of the land surface, and especially forests, in the earth's carbon cycle and climate. He is the Lead Scientist of the European Space Agency BIOMASS Mission, launching in 2022, which will measure forest biomass, height, and disturbance worldwide. He has published around

140 articles and written two books on radar, and has served on several national and international committees advising on climate and earth observation by satellites.



Maciej J. Soja (Member, IEEE) was born in Warsaw, Poland, in 1985. He received the B.Sc. degree in engineering physics, the M.Sc. degree in electrical engineering, and the Ph.D. degree in radio and space science from the Chalmers University of Technology, Gothenburg, Sweden, in 2008, 2009, and 2014, respectively.

Between 2014 and 2017, he was a Post-Doctoral Researcher and later a Research Assistant with Radar Remote Sensing Group, Chalmers University of Technology. Between 2017 and 2018, he was

a Senior Research Officer for Horizon Geoscience Consulting Pty. Ltd., Belrose, NSW, Australia. Since 2018, he has been the Director of MJ Soja Consulting, Hobart, TAS, Australia. He is also an Adjunct Researcher with the Discipline of Geography and Spatial Sciences, University of Tasmania, Hobart. His main research focus is synthetic aperture radar (SAR) mapping and monitoring of vegetation. Since 2009, he has been actively involved in the development of biomass estimation algorithms for the selected ESA P-band SAR mission BIOMASS. He has also participated in multiple EU and ESA projects, including Advanced SAR and GlobBiomass. He participated in the development of the tower radar experiment BorealScat and his research experience also includes electromagnetic modeling and laser scanning data analysis.



Lars M. H. Ulander (Fellow, IEEE) received the M.Sc. degree in engineering physics and the Ph.D. degree in electrical and computer engineering from the Chalmers University of Technology, Gothenburg, Sweden, in 1985 and 1991, respectively.

Since 2014, he has been a Professor in radar remote sensing with the Chalmers University of Technology. He also holds a part-time position at the Swedish Defence Research Agency (FOI), Linköping, Sweden, where he is the Director of research in radar signal processing and leads the research on VHF/UHF band radar. He has authored or coauthored over 300 professional publications, of which more than 70 are in peer-reviewed scientific journals. His research areas include radar imaging, synthetic aperture radar (SAR), signal processing, electromagnetic scattering models, and remote sensing applications.



Klaus Scipal (Member, IEEE) received the M.Sc. degree in geodesy and the Ph.D. degree in technical sciences from the Vienna University of Technology, Vienna, Austria, in 1999 and 2002, respectively.

He has been a Scientist with the Institute of Photogrammetry and Remote Sensing, Vienna University of Technology, and the European Centre for Medium-Range Weather Forecasts in the fields of earth observation and data assimilation with a focus on land surface processes. In 2009, he joined the Mission Science Division, European Space Agency, Noordwijk, The Netherlands, as a Mission Scientist working on the development of future SAR satellite systems. In 2020, he became a Mission Manager for the SMOS and BIOMASS satellite missions in the Mission Management Office, European Space Agency.